Fuel 201 (2017) 53–64

Contents lists available at ScienceDirect

Fuel

journal homepage: www.elsevier.com/locate/fuel

Full Length Article

An evaluation of the efficacy of various coal combustion models for predicting char burnout

Josh McConnell *, Babak Goshayeshi, James C. Sutherland

Department of Chemical Engineering, University of Utah, Salt Lake City, UT, United States

HIGHLIGHTS

- Evaluation of several coal combustion models with varying levels of fidelity.
- Effect of varying environmental parameters on burnout calculations investigated.
- Significant overlap in devolatilization and char oxidation is predicted.

ARTICLE INFO

Article history:
Received 24 May 2016
Received in revised form 9 November 2016
Accepted 15 November 2016
Available online 22 November 2016

Keywords:
Combustion
Coal
Simulation
Char oxidation

ABSTRACT

Coal combustion is comprised of several subprocesses including devolatilization and heterogeneous reactions of the coal char with O_2, CO_2, H_2O and potentially several other species. Much effort has been put forth to develop models for these processes which vary widely in both complexity and computational cost. This work investigates the efficacy of models for devolatilization and char reactions at either end of the complexity and cost spectrums for a range of particle sizes and furnace temperatures and across coal types. The overlap of simulated devolatilization and char consumption is also examined. In the gas phase, a detailed kinetics model based on a reduced version of the GRI 3.0 mechanism is used. The Char Conversion Kinetics and an n^{th}-order Langmuir-Hinshelwood models are considered for char oxidation. The Chemical Percolation and Devolatilization and a two-step model are considered for devolatilization. Results indicate that high-fidelity models perform better at representing particle temperature and mass data across a wide range of O_2 concentrations as well as coal types. A significant overlap in devolatilization and char consumption is observed for both char chemistry and devolatilization models.

1. Introduction

Coal combustion is a complex process that involves a number of highly-coupled physical phenomena, including reaction and transport of gas phase species, exchange of material between the gas and particle phases, and in many cases, the presence of turbulent flow. Modeling these processes, and their nonlinear interactions, in industrial-scale coal boilers poses a significant challenge. It is common practice to use empirical models for coal subprocesses in place of those with greater complexity [1–4], and even determine the beginning or end of some phenomena such as char oxidation *a priori* in order to reduce the computational load of performing needed calculations [2]. Furthermore, large variations in parameters such as particle diameter, furnace temperature, and oxygen concentration may occur within a single furnace. Therefore, it is important to know what effect these parameters have on quantities-of-interest such as particle mass and temperature over a range of model complexities, especially in the realm of char oxidation, which occurs over a much greater time span than evaporation and devolatilization.

Much effort has been put forth in development of char reaction models spanning a range of complexity. The simplest models use Arrhenius expressions that rely only on the partial pressure of species in the vicinity of the particle [1] and employ a global approach to the char reaction kinetics, while some go a step further and require calculation of surface partial pressures [5,6]. Yet more detailed models endeavor to resolve the physical subprocesses that occur during char oxidation and gasification. CBK-type models based on work by Hurt et al. [7], such as the CBK-E [8], and CBK-G [9] model char reaction kinetics based on the physical characteristics of the coal, and often include various submodels for evolution of particle diameter, char reactivity, and formation of an ash film. Possibly the most advanced CBK-type model is the Char Conversion Kinetics (CCK) model developed by Shurtz and Fletcher [10,11], which combines the gasification and oxidation kinetics of

* Corresponding author.
E-mail address: Josh.McConnell@chemeng.utah.edu (J. McConnell).

http://dx.doi.org/10.1016/j.fuel.2016.11.052
0016-2361/

[9,8] and considers Stefan flow. The most advanced approaches go as far as to discretize the char particle into concentric shells [12] or discrete cubical elements [13] in order to fully resolve intraparticle species transport and kinetics.

Some recent work has examined the efficacy of various char reaction models over a range of input parameters and simplifying assumptions. Maloney et al. [14] compare particle density and diameter calculations from the CBK model in 6 and 12 mol% oxygen environments, and compare predictions to experimental observations. It was concluded that the CBK model generally does a good job at predicting trends in particle diameter and density and that accurate input data on distributions of initial size and density are required for obtaining good predictions. Gonzalo-Tirado et al. [15] consider several approaches to modeling CO oxidation around burning char particles of various sizes. They conclude that use of a single film model yields acceptable error in temperature and mass calculations for particles with diameters less than 200 μm and that the choice of gas phase chemistry model significantly impacts the calculated particle temperature. Work by Goshayeshi and Sutherland [16] investigates the performance of various combinations of gas phase chemistry and coal devolatilization models over a range of furnace temperatures and particle diameters for laminar, single particle combustion, but focuses on ignition rather than char oxidation/gasification. It appears that there is a very limited body of work that explicitly addresses the potential overlap in devolatilization and oxidation physics and its effect on char burnout predictions. Work by Biagini and Tognotti [17] examine the reactivities of chars from various fuel sources and found that char reactivity is enhanced when devolatilization and char oxidation are allowed to occur simultaneously rather than strictly sequentially. McConnell and Sutherland [18] examine the importance of model fidelity in particle and gas phase chemistry models on char burnout calculations, and demonstrate that the choice of gas phase model has a substantial effect on particle temperature calculations and less so on predicted char burnout. Devolatilization kinetics were found to have an impact on char burnout calculations, but overlap of devolatilization and char oxidation was not explicitly addressed. It appears that only [10,11,19,18] publish particle temperature or mass calculations using CCK, and of these only [18] considers char oxidation. In two other studies, CCK is used only to estimate the effect of CO inhibition on CO_2 gasification of petroleum coke [20] and biochar [21].

The purpose of this study is to investigate the efficacy of two char reaction models: the CCK model which takes an intrinsic approach to modeling oxidation, and the n^{th}-order Langmuir-Hinshelwood model which uses a global rate expression. The effect of varying furnace temperature and initial particle diameter on calculations using either the CCK or LH models is examined. Calculated particle heating rates due to convection, heterogeneous reaction, and radiation are investigated. Additionally, the effect of devolatilization on particle temperature and mass calculations is investigated by employing two separate devolatilization models in tandem with CCK and LH models. To the authors' knowledge, this work is the first to analyze, in-depth, the effect of varying furnace temperature and particle diameter on char burnout calculations while spatially resolving gas-phase transport and kinetics and implementing high-fidelity models for homogeneous kinetics, devolatilization, and char consumption.

2. Theoretical formulation

2.1. Gas phase

The gas phase conservation equations are written in an Eulerian reference frame as [16,22]

$$\frac{\partial \rho\phi}{\partial t} = -\frac{\partial \rho\phi u}{\partial x} - \frac{\partial \Theta_\phi}{\partial x} + \omega_\phi + \sum_{j=1}^{n_p} \frac{S_{p_j\phi}}{V_{cell}}, \tag{1}$$

where ϕ is an intensive quantity, Θ_ϕ is the diffusive flux of ϕ, ω_ϕ is the net rate of production of ϕ in the gas phase, V_{cell} is the quantity representing the volume of the control volume, and $S_{p_j\phi}$ is gas-phase source term for ϕ from the particle phase. In this formulation, $\phi = \{1, u, v, e_0, Y_i\}$ where ρ is the mass density, u and v are the x and y components of velocity, respectively, e_0 is the specific total internal energy, and Y_i are species mass fractions. For the continuity equation, $\phi = 1$ and $\Theta_\rho = 0$.

2.2. Particle phase

Particle transport is accomplished using a Lagrangian frame of reference where position, velocity, diameter, temperature, mass, and composition are time-evolved for each particle. Two way coupling of particle velocity, composition, and temperature with the gas phase is considered. Gas displacement by the particle is neglected. Details of the formulation are available in [16,22].

2.3. Interphase coupling

Source terms for each species are calculated by summing contributions from evaporation, devolatilization, reactions with char. Evaporation and devolatilization terms are described in [16], while char reaction models are discussed in Sections 2.5.1 and 2.5.2.

The energy evolved due to char oxidation is determined by

$$\Delta H^{Ox} = \frac{\varphi \Delta H^{Ox}_{CO_2} + \Delta H^{Ox}_{CO}}{1+\varphi}, \tag{2}$$

where φ is the instantaneous ratio of CO_2 to CO produced through char oxidation. The source term in the particle energy balance is given as

$$S_r = \frac{1-\alpha}{m_p C_p}\left[\Delta H^{Evap}\left(\frac{dm_p}{dt}\right)^{Evap} + \Delta H^{Ox}\left(\frac{dm_c}{dt}\right)^{Ox} + \sum_k \Delta H^G_k \left(\frac{dm_c}{dt}\right)^G_k\right], \tag{3}$$

where m_p and m_c are the particle and char masses, respectively, and $k = \{CO_2, H_2O, H_2\}$. Superscripts "Evap," "Ox" and "G" denote evaporation, oxidation, and gasification, respectively. Enthalpies of reactions used for heterogeneous reactions with char have values $H^{Ox}_{CO_2} = -3.308 \times 10^4$, $H^{Ox}_{CO} = -9.630 \times 10^3$, $H^G_{CO_2} = 1.437 \times 10^4$, $H^G_{H_2O} = 1.094 \times 10^4$, and $H^G_{H_2} = -6.234 \times 10^3$ kJ/kg. The parameter α is the fraction of energy evolved from heterogeneous reactions that is transferred to the gas phase. In previous studies [16,22,18], we have used $\alpha = 0.3$ based on work by Gu et al. [23]. However, as mentioned in [18], a constant value for α does not yield accurate particle temperatures over a wide range of conditions. The authors recently proposed a model for α as [24]

$$\alpha = \frac{h_p r}{\kappa_p + h_p r}, \tag{4}$$

where $\kappa_p = D^T_p \rho_p C_p$ is the particle thermal conductivity, D^T_p and ρ_p are the particle thermal diffusivity and density, respectively. h_p is the convective heat transfer coefficient [16], and r is the particle radius. Eq. (4) attempts to model the competing effects of intraparticle and interphase energy transfer among the hot products of char combustion in the immediate (unresolved) vicinity of the particle, the gas phase, and the particle. Intraparticle and interphase heat transfer are represented by κ_p and $h_p r$, respectively.

2.4. Gas phase chemistry

A model based on the GRI 3.0 mechanism [25] consisting of 24 species and 86 reactions was used to solve for gas phase reactions. Tar devolatilized from the coal particle into the gas phase is assumed to have the empirical chemical formula $C_{10}H_8$. Soot, which is a product of tar cracking, is assumed to be composed purely of carbon. Gas phase reaction of tar and soot are considered through implementation of a model developed in [26]. CO and H_2O are assumed to be the only products of tar and soot combustion. Tar and soot chemistry is indirectly coupled to the implemented chemical mechanism through source terms for CO and H_2O resulting from tar and soot combustion. Transport equations for each species, with reactive and interphase source terms, are solved at each grid cell and for all times.

2.5. Coal submodels

To facilitate modeling, coal is assumed to be comprised of four constituents: moisture, volatiles, fixed carbon (*i.e.* char), and ash. Herein, time-evolution of moisture, volatiles, and char mass are considered. The ash mass within a coal particle is assumed to be constant in time.

The Two-Step (TS) [27] and Chemical Percolation and Devolatilization (CPD) [28] models are used to describe devolatilization. The Two-Step model assumes the devolatilized mass is composed of CO, H_2 and tar. Products evolved using CPD are CO, CO_2, CH_4, NH_3, HCN, H, H_2O and tar. For both devolatilization models, tar is assumed to be naphthalene. In this study, a comparison is made between particle temperature and mass calculations obtained using TS and CPD models.

Char oxidation and gasification are comprised of a multitude of heterogeneous reactions and depend on physical morphology, elemental composition of the ash, and a variety of other factors which have influence the transport and kinetic properties of the char. One approach to modeling char combustion is the inclusion of submodels for each physical process using the intrinsic properties of the coal. Another approach is use of empirical expressions that "absorb" the details of what is actually occurring. The CCK model [10], described in Section 2.5.1, takes the former approach, while the *n*th-order Langmuir-Hinshelwood model [5] described in Section 2.5.2, use the latter (and far simpler) approach to modeling char conversion.

2.5.1. CCK model

CCK implements the following overall heterogeneous chemistry

$$C_s + \frac{1}{2}\frac{1+2\varphi}{1+\varphi}O_2 \rightarrow \frac{1}{1+\varphi}CO + \frac{\varphi}{1+\varphi}CO_2, \quad (5)$$

$$C_s + H_2O \rightarrow CO + H_2, \quad (6)$$

$$C_s + CO_2 \rightarrow 2CO, \quad (7)$$

$$C_s + 2H_2 \rightarrow CH_4, \quad (8)$$

where φ is the molar ratio of CO_2 to CO production in Eq. (2). A three-step mechanism is used for (5), two-step reaction mechanisms are implemented for (6) and (7), and a single-step mechanism is used for (8), the details of which are provided in [10,9,8]. Rate constants for each reaction step are determined using $k_j = f_{RPM} f_T A_{j,0} \exp(-E_j/RT_p)$, where f_{RPM} is the ratio of current and initial internal surface area determined by the random pore model given in [29], and f_T is a factor which accounts for loss of active sites on the surface of the char due to annealing. Kinetic parameters are determined from correlations given in [8,9]. The value of f_T is calculated as [7]

$$f_T = \left(\int_0^\infty \theta \, dE_d\right)^{1/2}, \quad (9)$$

where θ is the mass-averaged fraction of active sites remaining on the char, and E_d is the activation energy for the annealing process. $\theta(E_d)$ is determined by

$$\frac{\partial \theta}{\partial t} = -f_{Dev} A_d \theta \exp\left(\frac{-E_d}{RT_p}\right), \quad (10)$$

where A_d is the annealing frequency factor, and f_{Dev} is a correction factor coupling the thermal annealing model to devolatilization,

$$f_{Dev} = \exp\left(-a[m_v/m_{v,0} - m_v]\right), \quad (11)$$

where $m_{v,0}$ is the initial mass of volatiles. The model for f_{Dev} is based neither on physical theory nor experimental observation and is included only as a means to prevent thermal annealing of the char during devolatilization. We have observed that, without such treatment, thermal annealing models become too aggressive at inhibiting char reactivity and burnout predictions are far below experimental observations. Realistically, several of the mechanisms responsible for the deactivation of coal char (*i.e.* thermal annealing) should not begin prior to its formation. Deactivation of char by thermal treatment is understood to be caused by the loss of active sites, loss of surface area, and loss of catalytic activity of inorganic material [7]. As devolatilization occurs, the coal undergoes a series of bridge-breaking and cross-linking reactions, so the reactivity of the coal matrix arguably increases (and eventually decreases) as devolatilization proceeds. In reality, "char" does not exist before devolatilization since it is the product of cross-linking reactions that occur among the organic constituents of the coal during pyrolysis [28]. Unfortunately, the coupling between char deactivation and devolatilization is poorly understood. Thus, further study of thermal deactivation of char during the devolatilization process is merited. In this study, $a = 30$ and θ is initialized to a lognormal distribution in E_d, with parameters as suggested in [7]. A detailed formulation of expressions for surface reaction rates for each species is given by [8–10].

A single film model is used for transport calculations from the bulk gas to the surface of the particle. The coupling between heterogeneous kinetics and intraparticle diffusion is modeled through effectiveness factors for each surface reaction. An ash film growth model as well as mode-of-burning relations, which relate the particle diameter and density, are taken from [7]. Because heterogeneous kinetics depend on the concentration of the reacting species at the particle surface, solving the following expression is required

$$P_{i,s} = \begin{cases} \frac{P}{\gamma_i}\left[1 - \left(1 - \gamma_i \frac{P_i}{P}\right) \times \exp\left(-\frac{\gamma_i q_i R T_m}{h_i P}\right)\right] & \gamma_i \neq 0 \\ P_i + \frac{q_i R T_m}{h_i} & \text{otherwise} \end{cases}, \quad (12)$$

where P_i^s and P_i are the surface and bulk partial pressures of species, i, respectively, γ_i accounts for Stefan flow, q_i is the flux of species i at the particle surface, T_m is the arithmetic mean of the particle and interpolated gas temperatures, and h_i is the mass transfer coefficient for species i computed by the method described in [30]. The species mass fluxes, q_i are calculated by equating the rate of mass transfer to the net rate of production per unit surface area of the particle for each species, and solving the resulting nonlinear system of equations. The details of constructing this system are given in Section 6.2 of [10]. The species source terms due to reactions with the char are calculated as $(dm_c/dt)_i = \pi d_p^2 M_i q_i$, where $i = \{CO_2, CO, O_2, H_2, H_2O, CH_4\}$ and M_i is the molecular weight of species i.

The overall rate of char depletion is calculated as

$$\frac{dm_c}{dt} = \left(\frac{dm_c}{dt}\right)^{Ox} - \sum_j \frac{M_c}{\nu_j^G M_j}\left(\frac{dm_j}{dt}\right)^G, \quad (13)$$

where $j = \{CO_2, H_2O, H_2\}$, m_j is the mass of species j, and v_i denotes the moles of species i produced per mole of char reacted with species i. The quantity φ is obtained directly from the oxidation kinetics in CCK, and is given as $\varphi = k_1 c_{O_2,s}/k_2$,where $c_{O_2,s}$ is the concentration of O_2 at the char surface and k_1 and k_2 are the rate constants corresponding to the rates expressions for CO_2 and CO production, respectively. The particle diameter is determined by the mode of burning relations described in [7], consistent with many implementations of CBK-type models [8–10].

2.5.2. n^{th}-order Langmuir-Hinshelwood

In addition to the CCK model, an n^{th}-order Langmuir-Hinshelwood (LH) model developed in [5] was implemented for char oxidation calculations:

$$q_{O_2} = \frac{k_2 k_1 P_{O_2,s}^n}{k_1 P_{O_2,s}^n + k_2}, \tag{14}$$

where q_{O_2} is the flux of O_2 at the surface of the particle. The ratio of CO_2 and CO produced via oxidation is calculated by [31]

$$\varphi = 0.02 P_{O_2,s}^{0.21} \exp\left(-3070/T_p\right), \tag{15}$$

where T and $P_{O_2,s}$ have units K and atm, respectively. The partial pressure of O_2 was determined using the film diffusion model described in [5]. Activation energies used to calculate k_2 and k_1 are taken from [5] and are assumed to have units J/mol instead of kJ/mol. This assumption was necessary to reproduce the predicted char burning rates presented in [5]. Char gasification is determined using first-order Arrhenius expressions

$$q_j^G = P_{j,s} A_j \exp\left(-E_j/RT_p\right), \tag{16}$$

to determine the production rates of species $j = \{CO_2, H_2O\}$ by gasification. The Arrhenius parameters used for gasification are taken from [11,19]. The LH model, used in tandem with (16) accounts for reactions (5)–(7). Species mass production rates and the mass of char lost through oxidation are calculated in the manner described in Section 2.5.1. The overall char consumption was calculated using (13) with $j = \{CO_2, H_2O\}$. Unlike the CCK model, where the particle diameter changes, it is assumed to be constant for the LH model, with the particle density decreasing in time.

3. Computational setup

The computational configuration emulates the entrained-flow laminar reactor where single particle combustion was examined, as described in [5] and is illustrated in Fig. 1. These data were chosen because they were collected under conditions in which raw coal undergoes both devolatilization and heterogeneous oxidation, which represents combustion within a commercial system more accurately than systems in which only char oxidation occurs.

The governing equations are solved using a fully-coupled scheme with a second order spatial discretization, explicit time integration, and characteristic boundary conditions [32]. The computational domain is 1.4 cm in length with a grid spacing of 140 μm and a time-step of 80 ns. The domain is aligned in the x-direction and moves in the y-direction according to a mean system velocity [33]. The x-axis is perpendicular to the main flow direction and the y-axis is parallel to the main flow direction. For all calculations, a single particle is placed at the domain center. Although displacement of fluid by the particle is neglected, source terms to and from the particle take into account the particle's finite size. If the particle overlaps multiple grid cells, source terms are distributed among those cells. The complete combustion process (devolatilization through char burnout) is considered for a subbituminous coal (Highvale) and a bituminous coal (Eastern Bituminous), at four oxygen mole fractions (0.06, 0.12, 0.24, and 0.36). Simulations are also carried out for the Eastern Bituminous coal using 3 additional O_2 mole fractions (0.48, 0.60, and 0.72), although no experimental data is available in [5] for oxygen mole fractions exceeding 0.36. The proximate and ultimate analyses of the coals used are given in Table 1. In all cases, mole fractions of H_2O, and CO_2 are initialized to 0.14 and 0.04, respectively, with the balance being N_2. For all calculations the initial particle temperature and density are set to 350 K and 1200 kg/m^3, respectively. Unless otherwise specified, the initial gas temperature was set to 1685 K, consistent with experimental conditions corresponding to an adiabatic flame temperature T_{ad}=1800 K.

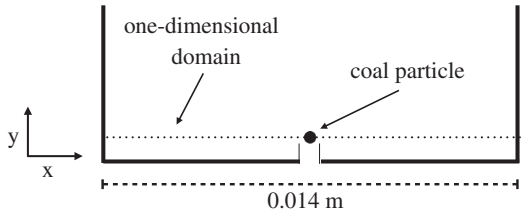

Fig. 1. A schematic of the system considered.

The computational configuration used in this work sacrifices dimensionality (1D instead of 2D or 3D) to allow for tractable calculation of gas phase transport and chemical kinetics over a wide range of parameters. Furthermore, particles do not displace fluid volume (although they are coupled to grid cells that they overlap) which precludes resolution of particle boundary layers. Because species gradients within the immediate vicinity of the particle are not necessarily resolved, a film diffusion model is employed for both char models investigated. These are all limitations of the present modeling approach. Particle-resolved DNS would be required to completely characterize the thermochemical and transport processes involved, which is beyond the scope of this work. However, results presented here are grid-converged; simulations performed on a domain with finer grid spacing yield the same particle temperature and mass histories.

4. Results and discussion

Simulations were carried out to assess the accuracy of particle temperature and mass calculations using two approaches for devolatilization and char consumption at four oxygen concentrations for two coal types. Furthermore, the effect of varying initial particle diameter and furnace temperature on particle temperature and mass predictions is investigated. Burnout calculations are compared to experimental observations where available. All results shown herein are truncated at the time at which complete char burnout is calculated to occur.

4.1. Evaluation of CCK and LH models

In this section, particle temperature and mass calculations resulting from the CCK and LH models are compared to experimental observations in order to assess the accuracy of each model.

Fig. 2 depicts particle temperature and fractional dry, ash-free (DAF) mass as calculated using the CCK and LH models using CPD for devolatilization. The CCK model represents DAF particle mass evolution more accurately than the LH model for the Eastern Bituminous coal, as demonstrated by Fig. 2. Predicted DAF mass histories computed by the CCK model follow experimental data fairly well for Eastern Bituminous coal at 12%, 24%, and 36% O_2. However, CCK significantly over-predicts the DAF mass remaining at residence times exceeding 80 ms for 6% O_2. The LH model also

Table 1
Proximate and ultimate analyses of Eastern Bituminous and Highvale coals.

	Proximate %				Ultimate (dry) %				
	Moisture	Ash	Volatile	Fixed C	C	H	O	N	S
Eastern Bituminous	0.75	8.82	34.91	55.52	84.87	5.57	6.92	1.59	1.05
Highvale	7.61	11.39	37.15	43.89	69.23	4.57	24.93	0.95	0.32

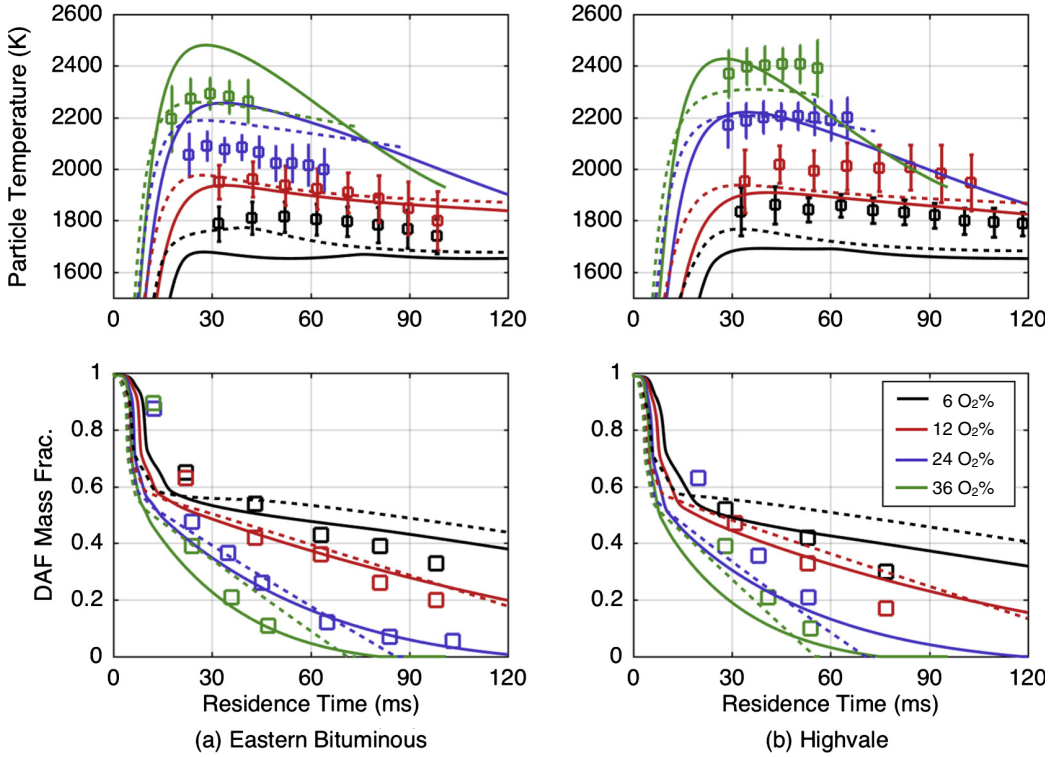

Fig. 2. Particle temperature and dry, ash free (DAF) mass histories resulting from the CCK (solid) and LH (dotted) models Eastern Bituminous and Highvale coals. CPD is used for devolatilization. Experimental data are represented by open squares with vertical bars indicating one standard deviation.

represents Eastern Bituminous DAF mass data fairly well, but not quite as well as CCK with the exception of the 12% O_2 data set where mass curves for either char model are nearly indistinguishable. For the most part, while CCK and LH capture the general trend for DAF with Highvale coal, neither produces the same level of quantitative agreement with experimental data that is seen with the Eastern Bituminous coal. In low O_2 ($\leqslant$12%) environments, the CCK model produces DAF mass histories that more accurately represent experimental values for the Highvale cool than the LH model, however both models tend to underestimate DAF mass loss. Both models overestimate the mass loss at 24% and 36% O_2, especially at residence times less than 35 ms, with the LH model performing better than CCK. One reason the CCK model fails to accurately represent the mass data of the Highvale coal at elevated O_2 environments is that the kinetic parameters used for oxidation calculations likely misrepresent the reactivity of Highvale coal char. The char burnout data used to develop the correlation used to determine rate constants for the char oxidation reactions span a DAF C% of 75–91% for atmospheric pressure [8]. Furthermore, the correlation used to calculate char oxidation kinetics predict that reactivity increases exponentially as DAF C decreases. At 69% DAF C, the Highvale coal is well below the range that this correlation should be applied with confidence. Thus, it is very likely that the kinetic parameters used in the CCK model overestimate the reactivity of Highvale coal char with oxygen. This assessment agrees with the mass calculations resulting from the CCK at 24% and 36% O_2.

Fig. 2 also indicates that the qualitative behavior of the predicted mass histories is dependent on the chosen char chemistry model, especially at elevated O_2 concentrations. At 6% and 12% O_2, both the LH and CCK models yield DAF mass histories that are approximately linear post-devolatilization for both coal types considered. However, the behavior of DAF mass predictions for both char models diverge at elevated O_2 concentrations. At 24% and 36% O_2, DAF mass histories predicted by the CCK model are distinctly concave up, whereas the LH model predicts a linear DAF mass history post-devolatilization. The authors of [5] compare measured reaction rates to calculated diffusion limitations which suggest that char combustion in low O_2 environments ($\leqslant$12 mol %) is diffusion limited at the furnace temperatures considered. However, it is also observed in [5] that as the ambient oxygen concentration is increased, film diffusion limitations are diminished. Due to the diffusion limitations exhibited by the experimental data described in [5], one might expect that calculations of the char consumption rate would be independent of the chosen char reaction model at low O_2 concentrations and at sufficiently high temperatures. This is exactly what is observed in the DAF mass calculations presented in Fig. 2.

At elevated oxygen concentrations, the CCK model produces particle mass histories that gradually level off with increasing

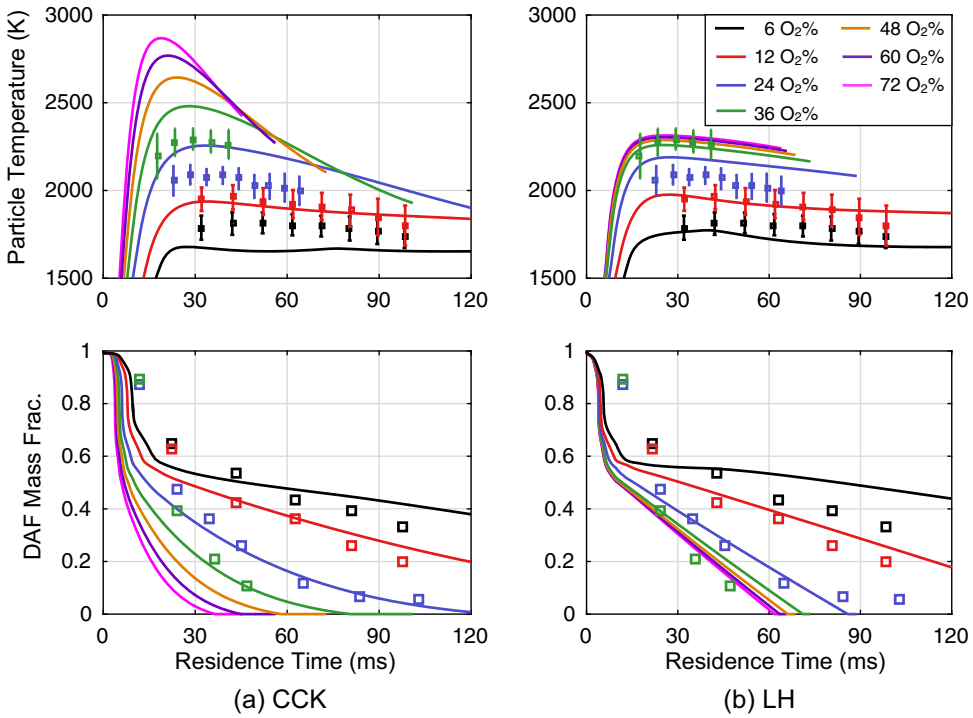

Fig. 3. Particle temperature and dry, ash free (DAF) mass histories resulting from the CCK (left) and LH (right) models for Eastern Bituminous coal for 6–72 mol% O_2. Experimental data for 6–36% O_2 are represented by open squares with vertical bars indicating one standard deviation. CPD is used for devolatilization.

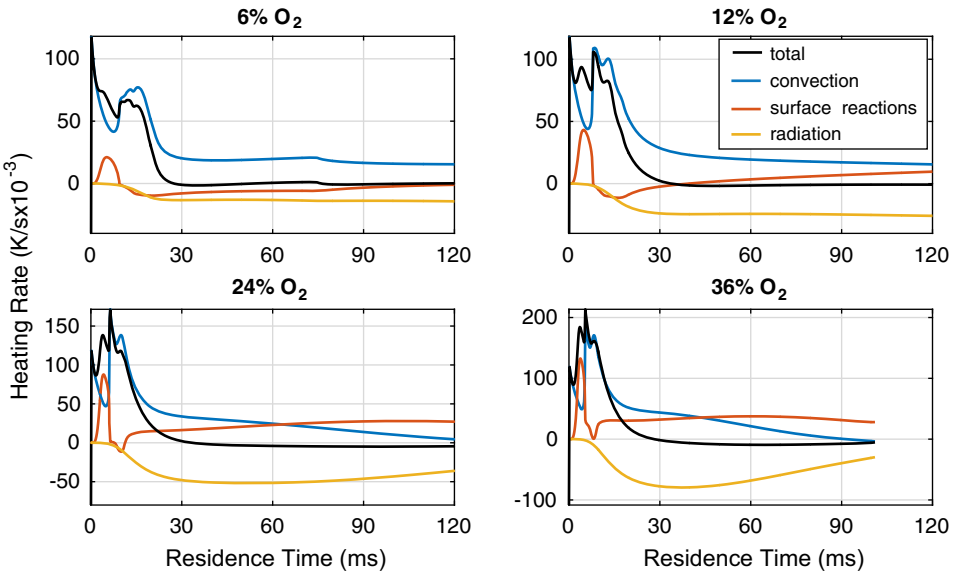

Fig. 4. Breakdown of heating rates calculated using the CCK model under all O_2 environments considered for the Eastern Bituminous coal. CPD is used for devolatilization. Heating rates due to convection, surface reactions, and radiation are shown along with the total particle heating rate.

residence time which is primarily due to the inhibiting effects of a growing ash film, as predicted by the ash inhibition model included in the CCK model. Mass calculations resulting from the LH model are nearly linear post-devolatilization. The observed qualitative differences between the particle mass calculations resulting from the CCK and LH model suggest that char combustion becomes less diffusion limited at 24% and 36% O_2, which is in agreement with the analysis in [5].

As Fig. 2 shows, Both models struggle to capture the temperature over the full range of O_2 concentration, with CCK showing a larger variance in temperature over the O_2 range considered here. For both coal types, particle temperatures resulting from the CCK model at 6% and 12% O_2 are lower than those predicted by the LH model. For the Eastern Bituminous coal, the CCK model underestimates the particle temperature by approximately 100 K for the 6% O_2 environment, and overestimates by as much as 200 K for 24% and 36% O_2. However, CCK accurately reproduces particle temperatures measured in 12% O_2 conditions.

Calculations similar to those illustrated in Fig. 2 are shown in [18], however, calculations in [18] use the full GRI 3.0 mechanism

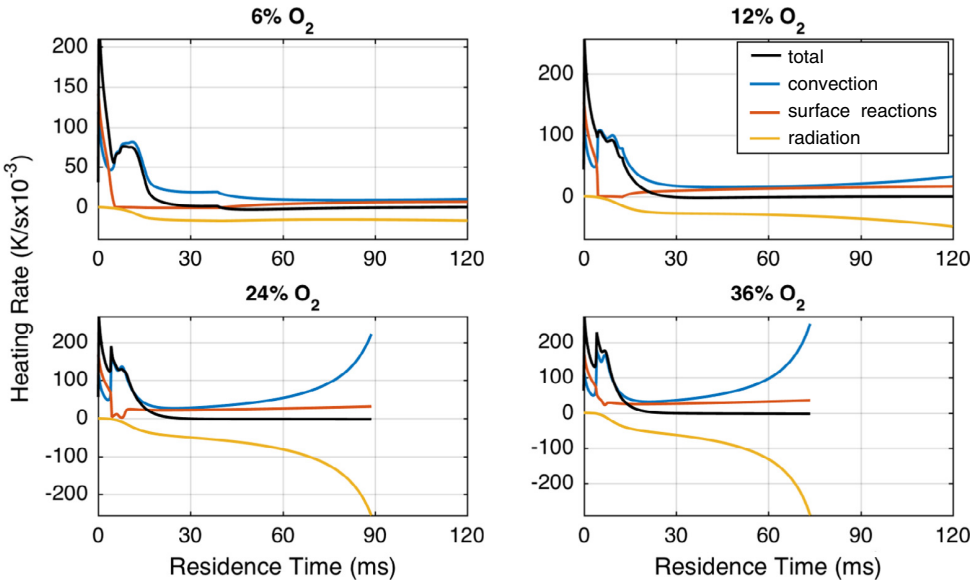

Fig. 5. Breakdown of heating rates calculated using the LH model under all O_2 environments considered for the Eastern Bituminous coal. CPD is used for devolatilization. Format is identical to that of Fig. 4.

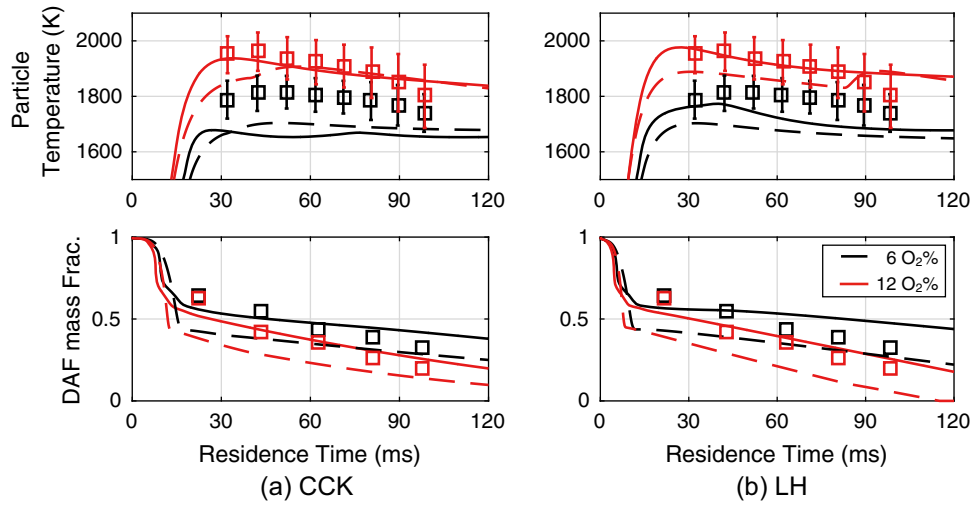

Fig. 6. Particle temperature and mass predictions for Eastern Bituminous coal resulting from (a) CCK and (b) LH char models using CPD (solid lines) and TS (dotted lines) for devolatilization. Open squares are experimental observations.

which implements 325 reactions for 24 species and imposes a constant value of 0.3 on α. Predictions for DAF particle mass presented in Fig. 2 do not differ significantly from analogous predictions shown in [18], but particle temperature calculations presented here better agree with experiments than temperature calculations in [18].

Fig. 3 shows particle temperature and DAF mass as calculated using the CCK and LH models for oxygen concentrations ranging from 6–72% where CPD is employed for devolatilization. Although data for particle temperature and DAF mass are not available for oxygen concentrations beyond 36% O_2, Fig. 3 provides some insight into the behavior of the LH and CCK models at oxygen concentrations as high as 72%. For both char LH and CCK models investigated, the peak particle temperatures and time to complete char burnout monotonically increase and decrease with increasing oxygen concentration, respectively. As Fig. 3 demonstrates, the DAF mass and particle temperatures predicted by the CCK model are significantly more sensitive to O_2 concentration at and above 36%. The particle temperature and DAF mass predicted by the LH model for environmental O_2 concentrations becomes difficult to distinguish beyond 24% O_2 suggesting that LH predicts kinetically-controlled char combustion at oxygen concentrations at 36% and higher. Conversely, DAF particle mass and temperature histories predicted by CCK for O_2 concentrations at or exceeding 36% are readily distinguishable. This result indicates CCK predicts that char oxidation is under diffusion control at O_2 concentrations exceeding 36%. In the absence of data, it is not possible to determine whether CCK or LH provides more appropriate trends for DAF mass and particle temperature under O_2 concentrations beyond 36%. However, for the data that does exist, CCK matches the trend much better than LH.

Figs. 4 and 5 show a breakdown of the particle heating rates for the Eastern Bituminous coal using CCK and LH models, respectively, at all O_2 concentrations considered. At early residence times,

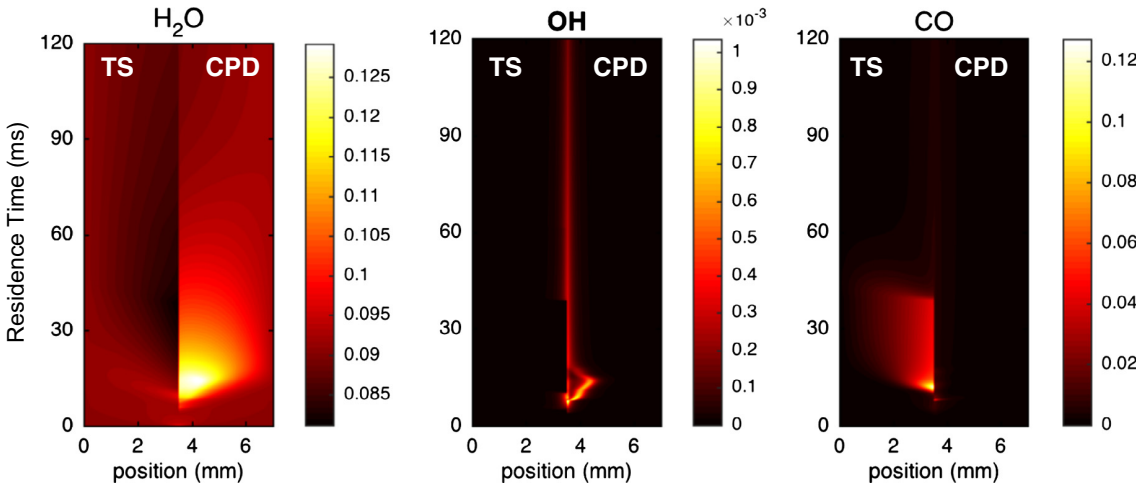

Fig. 7. Mass fractions for H_2O, OH, and CO for the Eastern Bituminous coal at 12% O_2. Mass fractions resulting from the TS and CPD models are given in the left and right halves of each plot, respectively. CCK is used for reactions with the char.

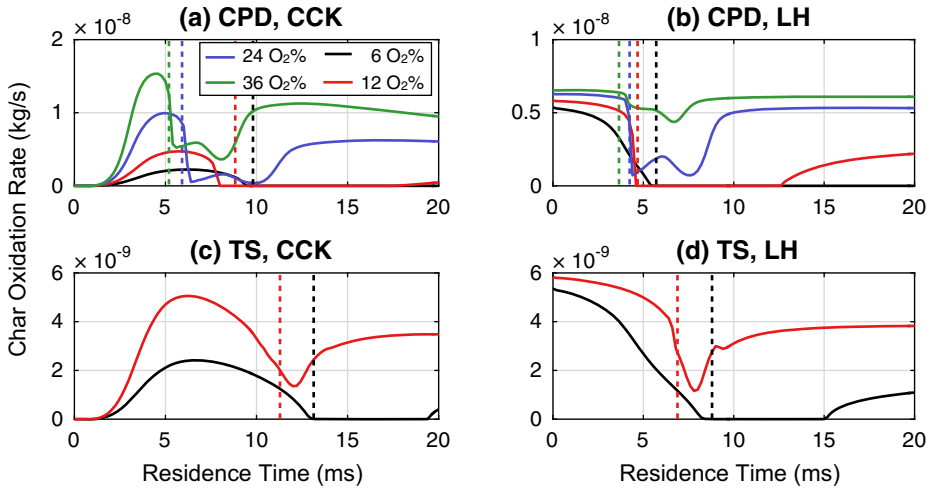

Fig. 8. Char oxidation rates using (a) CPD/CCK, (b) CPD/LH, (c) TS/CCK, and (d) TS/LH for devolatilization/char oxidation over a range of oxygen concentrations. Vertical lines indicate the residence times at which half of the volatiles remain.

some very peculiar behavior occurs for the convective and reactive contributions to the particle heating rates for both char models. The CCK model indicates that initial heating of the particle is dominated by convective heat transfer from the gas to the particle. However, the breakdown of heating rates for the LH model indicates that heating due to heterogeneous reactions is non-zero initially, and is actually larger than the heating rate due to convection. This prediction is unrealistic given that T_p is set to 350 K initially, which is well below the autoignition temperature of coal char. The occurrence of char oxidation at the beginning of simulations implementing the LH model is due to the fact that activation energies used with Langmuir-Hinshelwood expression for char oxidation are unrealistically small (< 1.1 kJ/mol). In [5], the authors state that all burnout calculations LH model were done for devolatilized coal. As a result, observing the prediction of char rapidly oxidizing at 350 K was precluded. As mentioned in Section 2.5.2, activation energies in [5] were assumed to have units J/mol since calculated char burning rates could not be reproduced with the published units kJ/mol. Burn rates using the published units were significantly lower than those calculated in [5] even under the assumption of complete kinetic control ($P_{O_2,s} = P_{O_2}$).

For the LH model at 24% and 36% O_2, the heating rate due to convection and radiation sharply rise and fall, respectively, at residence times approaching complete char burnout. This behavior is due to a reduction in C_p caused by the depletion of char, which has a significantly higher heat capacity than ash. Similar spikes in the convective and radiative heating rates are not observed for the CCK model because the reduction of the particle radius as complete burnout is approached reduces the convective and radiative heat transfer to and from the particle which counteracts the decrease in C_p.

4.2. Comparison of CPD and two-step devolatilization models

In this section, the Two-Step (TS) and CPD devolatilization models are used in combination with either LH or CCK for char chemistry. Only 6% and 12% oxygen environments are considered for the TS model because the time-step required to satisfy stability for the gas phase chemistry under 24 and 36% O_2 conditions is prohibitively small. The increased stiffness is due to the large amount of H_2 predicted to evolve by the TS model. Fig. 6 shows particle temperature and DAF mass predictions for the Eastern Bituminous

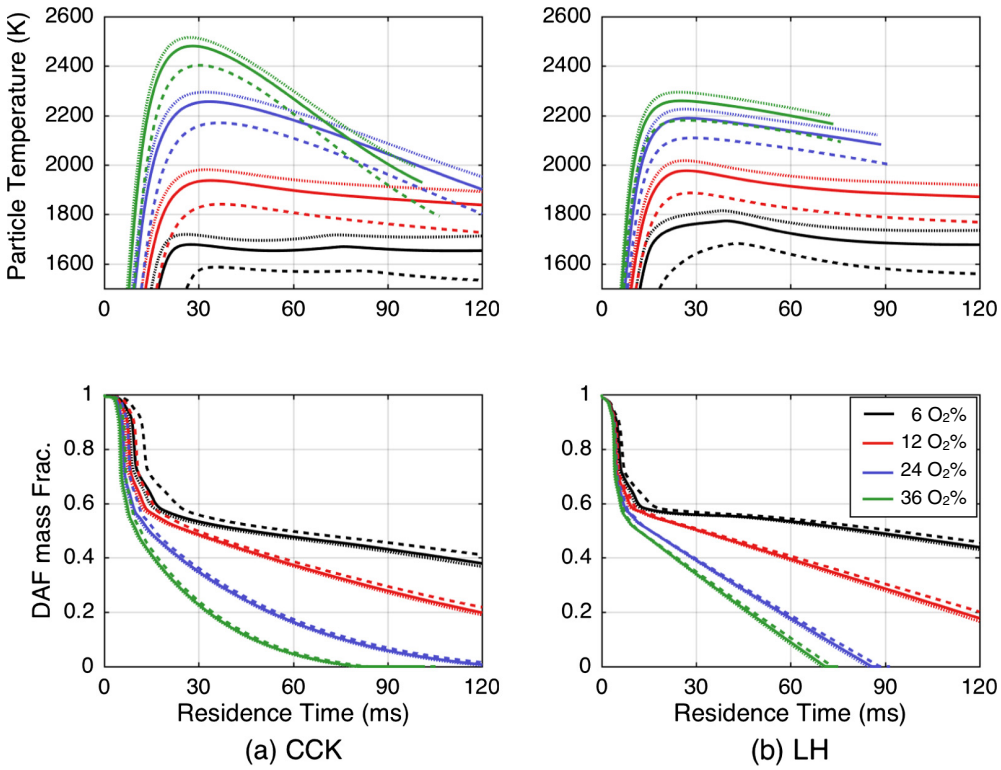

Fig. 9. Plots of particle temperature and mass histories for $T_{g,0}$ set to 1440 K (dashed), 1686 K (solid), and 1800 K (dotted) obtained using the CCK and LH models for the Eastern Bituminous coal. CPD is used for devolatilization.

coal resulting from using CCK and LH char models and CPD and TS devolatilization models in 6% and 12% O_2 environments. Particle temperature and mass histories calculated using CPD for devolatilization are closer to experimental values compared to when the TS model is used for both char reaction models considered. In all cases, the TS model predicts DAF masses that are substantially lower than values predicted when the CPD model is in use. This is because the TS model predicts that a fraction of the fixed carbon (char) within the coal is lost to devolatilization at high temperatures.

Fig. 7 shows contours of H_2O, OH, and CO mass fractions for the Eastern Bituminous coal over the spacial domain and residence time for both devolatilization models used with CCK for char kinetics. When either char model is used, the maximum gas phase temperature (which occurs just after ignition of the devolatilized matter) is approximately 200 K and 150 K less for 6% and 12% O_2 environments, respectively. The observed drop in peak gas temperature when the TS devolatilization model is used over CPD appears to be due to accumulation of CO in the gas phase. Homogeneous combustion of CO occurs mainly through two mechanisms: a "wet" mechanism, which involves reaction of CO with OH, and a "dry" mechanism in which no hydrogen-containing species participate [34]. The "wet" CO combustion is much faster than the "dry" mechanism. As Fig. 7 shows, CPD predicts significantly more H_2O as a combustion product of coal volatiles than TS, which has some influential consequences. First, the rate of steam gasification predicted when CPD is used is nearly 2× the rate when TS is used. Second, the availability of OH for reaction with CO is much higher when CPD is used, so CO evolved from the particle is predicted to combust much faster than for TS devolatilization. As a result of the more rapid CO combustion, the peak gas temperature is higher when CPD is used over the TS model independent of the implemented char model or oxygen concentration. The incidence of higher T_g values is the primary factor behind the higher T_p observed for when CPD/LH is used for devolatilization/char oxidation over TS/LH at 6% and 12% O_2 Although the calculated T_g is higher for all cases in which CPD is used over TS, the enhanced rate of steam gasification (due to the higher predicted H_2O concentration) is enough to counteract the rise in convective heat transfer when CCK is implemented. Moreover, some peculiar behavior for the OH mass fraction occurs when the TS model is implemented. At around 10 ms, an abrupt decrease in the mass fraction of OH is observed which is caused primarily by sharp increase in the mass fraction of CO (which readily reacts with OH) that occurs at the same time. After this, a sustained period of very low OH mass fraction from 10–40 ms is caused by the relatively high concentration of CO. The rather sudden increase in OH at around 40 ms is due largely to the sharp reduction of CO at about the same residence time.

Fig. 8 shows char oxidation rates using combinations of TS/CPD and LH/CCK across various oxygen concentrations. Vertical dotted lines indicate the time at which half the volatiles remain in the coal particle. For all model combinations and O_2 concentrations shown in Fig. 8, appreciable char oxidation occurs before half of the volatiles have been consumed. This suggests that heterogeneous oxidation may enhance the process of devolatilization, even at low (6%) oxygen concentrations.

As Fig. 8 illustrates, the LH model developed in [5] predicts char oxidation at the initial state, which, as discussed in Section 4.1, is not physically realistic, and is the main contributor to the qualitative differences in the oxidation behavior predicted by the LH and CCK models. Activation energies provided in [5] were assumed to have units J/kg instead of kJ/kg, which was required to reproduce the char burning rates in [5], and is the reason char oxidation is observed at the initial state. To a far lesser extent, the thermal annealing model in the CCK also contributes to the qualitative

differences in the calculated char oxidation rates. Nonetheless, the predicted overlap in devolatilization and char oxidation indicates that neither the LH or CCK are physically representative of the heterogeneous chemistry that may occur during the devolatilization process, as both assume reaction only with amorphous carbon. However, devolatilization occurs over a much shorter time frame than char oxidation so the physical correctness of a char chemistry model when volatiles are present is likely of little consequence under oxidative conditions.

4.3. Impact of varying initial furnace temperature

To investigate the effect of initial furnace temperature, $T_{g,0}$, on particle DAF mass and temperature calculations, simulations were run with $T_{g,0}$ set to 1440 K, 1685 K, and 1800 K (corresponding to adiabatic flame temperatures, T_{ad} equal to 1600 K, 1800 K, and 2000 K, respectively) which are the approximate values for the gas temperatures at the reactor inlet for experiments described in [5]. Particle temperature and mass data corresponding to T_{ad} = 1600 K and 2000 K was unpublished and not otherwise available. Nonetheless, according to one of the authors of [5], particle temperature measurements did not vary appreciably among experiments run at various furnace temperatures [35]. Unfortunately, no information was provided regarding DAF mass data for the T_{ad} = 1600 K and 2000 K data sets.

Fig. 9 shows calculated particle temperatures and fractional DAF mass using three initial furnace temperatures using the CCK and LH models for the Eastern Bituminous coal. The DAF mass is only weakly dependent on $T_{g,0}$ over the majority of each simulation when either of the char models is used, and this dependence weakens with increasing bulk oxygen concentration as Fig. 9 illustrates. The only cases in which the calculated DAF mass varies significantly over the values of $T_{g,0}$ considered are those with 6% O_2 environments, specifically at early residence times (during devolatilization). For both CCK and LH, the majority of the calculated mass differences across values of $T_{g,0}$ is due to differences in the volatile mass loss. The relatively high sensitivity of the DAF mass to $T_{g,0}$ for 6% O_2 is due to a number factors. First, the rate at which devolatilization and heterogeneous reactions occur is highly dependent on the particle temperature which, in turn, is dependent on the gas temperature in the vicinity of the coal particle. Furthermore, the diffusivity of gaseous species and the rates at which gas phase reactions occur increase as the temperature is elevated. As a result, the rate at which heat is evolved from combustion of devolatilized matter increases, which increases convective heat transfer to the devolatilizing coal particle. These factors are more pronounced at 6% O_2 than the other oxygen concentrations considered because combustion of devolatilized matter is more diffusion-controlled in low oxygen environments.

As Fig. 9 illustrates, the calculated particle temperature histories exhibit greater dependence on $T_{g,0}$ than DAF histories do, but show only moderate sensitivity. Similar to the DAF mass profiles, the particle temperatures become less sensitive to the initial furnace temperature as the bulk oxygen concentration is increased.

4.4. Impact of varying initial particle diameter

To observe the effect of varying initial particle diameter, simulations were carried out setting $d_{p,0}$ to 95, 115, and 135 μm. The intermediate value corresponds to the geometric mean of the sieved size fraction (106–125 μm) used in experiments [5]; coincidentally, it is nearly equal to the value of the arithmetic mean (116 μm). In [5], it is noted that standard deviations of measured particle sizes ranged from 20 to 35 μm. The smallest and largest values of $d_{p,0}$ were chosen to be 20 μm smaller and larger than the intermediate value because standard deviations of the particle size measurements taken at early residence times were typically 20 μm for data originating from the study described in [5]. Fig. 10 shows particle DAF mass histories for CCK and LH models paired with CPD for $d_{p,0}$ = 95, 115 and 135 μm across all O_2 concentrations considered. For all calculations shown in Fig. 10, the rate at which the normalized DAF mass is depleted increases as $d_{p,0}$ is decreased. For a given $d_{p,0}$, DAF mass profiles calculated using the CCK and LH models follow very similar trends at the lowest O_2 concentration. As Fig. 10 illustrates, the behavior of the DAF mass histories becomes increasingly dissimilar as the environmental O_2 concentration is increased and as $d_{p,0}$ is decreased. The observed divergence in behavior is caused by a decline in the mass

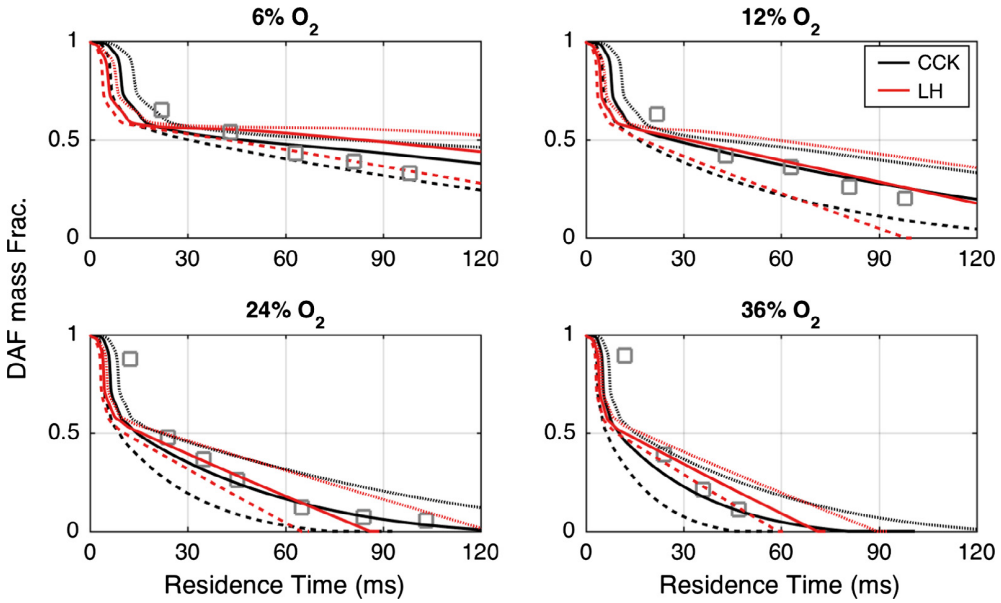

Fig. 10. Calculated particle DAF mass for CCK and LH models with $d_{p,0}$ set to 95 μm (dashed), 115 μm (solid), and 135 μm (dotted) for the Eastern Bituminous coal. CPD is used for devolatilization.

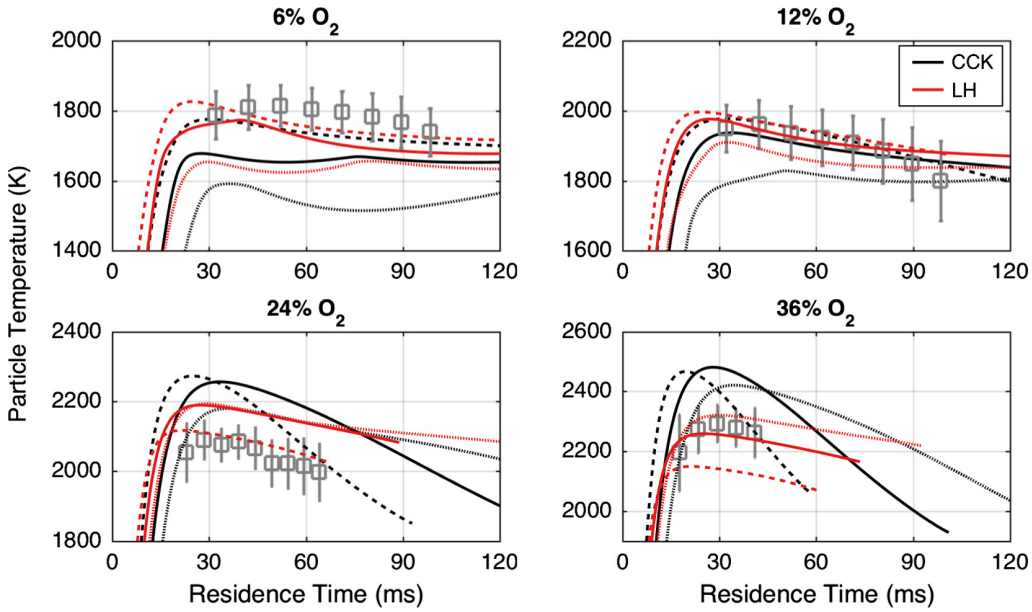

Fig. 11. Particle temperature histories resulting from the CCK and LH models with $d_{p,0}$ set to 95 μm (dashed), 115 μm (solid), and 135 μm (dotted) for the Eastern Bituminous coal. CPD is used for devolatilization. Grey boxes with vertical bars denote experimental data and ± one standard deviation range.

transfer limitations as the particle size is decreased and, as mentioned in Section 2.5.1, as the environmental O_2 concentration is increased.

Fig. 11 shows the evolution of particle temperature for CCK and LH models with $d_{p,0}$ = 95, 115 and 135 μm across all oxygen environments considered. The T_p histories are strongly influenced by $d_{p,0}$ over the range of oxygen concentrations considered. For both CCK and LH models, the peak particle temperature increases with decreasing $d_{p,0}$ for 12% and 6% O_2. This trend holds true for 24% O_2 environments, but breaks down at 36% O_2. Peaks in the particle temperature become more broad as the $d_{p,0}$ is increased with the CCK model. This tendency becomes more pronounced with increasing oxygen concentrations. At elevated oxygen concentrations, trends for the calculated particle temperature visibly change for both char chemistry models. At the 24% O_2 condition and using the LH model, particle temperature curves for $d_{p,0}$ equal to 115 and 135 μm are nearly indistinguishable before complete char burnout. Furthermore, the maximum value of T_p for $d_{p,0}$ = 95 μm is the lowest of all initial particle sizes considered. Additionally, maximum T_p increases as $d_{p,0}$ is increased using LH, which is exactly the opposite of the trend observed for 6% and 12% oxygen environments.

The relationship between T_p and $d_{p,0}$ is governed by several factors that scale differently with d_p. For instance, the amount of volatiles and thermal inertia scale with d_p^3 while surface reaction rates and heat transfer to and from the particle scale with d_p^2. The consequence of the difference in the scaling of these quantities varies with the available O_2. In low O_2 environments, release of volatiles quickly depletes the oxygen near the simulated coal particle by means of displacement and combustion reactions; this has the effect of attenuating char oxidation, which is the sole source of energy post-devolatilization. Additionally, energy transfer due to convection and char oxidation, (both are positive at all residence times for all oxygen concentrations considered), scale with external particle surface area, and thermal inertia scales with the particle mass which works to decrease the particle heating rate and thus T_p. At elevated O_2 environments, depletion of oxygen near the particle through devolatilization and homogeneous combustion becomes less of an issue for all $d_{p,0}$. Instead, heat loss through radiation increasingly determines the trends for T_p with changing $d_{p,0}$ for 24% and 36% O_2, which is especially the case for the LH model as it assumes a constant particle diameter. Other factors accounted for in the CCK, such as ash film growth and particle shrinkage, change the mass transfer characteristics of the particle and play an important role in the how the shape evolves as $d_{p,0}$ and O_2 concentration is varied.

Although the simulations presented above resolve gas phase species transport and chemical kinetics, diffusion through a boundary layer surrounding the particle is not properly resolved and is instead modeled using a single-film approach. However, a study [36] comparing several film diffusion models to a film-resolved calculation in a series of char combustion simulations concludes that the single-film approach adequately describes species transport through a particle boundary layer. Furthermore, species transport within the porous structure of the coal particle is not resolved and is either explicitly modeled through calculation of effectiveness factors, as was done with CCK, or is "absorbed" into the heterogeneous chemistry model, which is the approach used with LH. Clearly, these are limitations to the modeling approach. However, determining the exact implications of modeling versus resolving boundary layer and intraparticle species transport is beyond the scope of this work.

5. Conclusion

In this work, several combinations of char reaction (CCK and LH) and devolatilization (CPD and TS) models with differing levels of complexity are compared across two coal types and a range of oxygen concentrations. Results indicate that both char models perform similarly for 6 and 12% O_2 independent of coal type and devolatilization model, although CCK does a somewhat better job predicting particle mass histories while the LH model is better at predicting the particle temperature. At higher oxygen concentrations, the accuracy of LH model is hit or miss with respect to the particle temperature and represents experimental observations for the particle mass less accurately than CCK for both coal types.

Mass predictions resulting from the CCK model match experimental trends quite well, but particle temperatures overestimated by as much as 200 K for the Eastern Bituminous coal. However, CCK overestimates mass loss for the Highvale coal in elevated oxygen environments. This is likely because correlations for the kinetic parameters greatly overestimate the reactivity of Highvale char, and because a shift away from bulk diffusion control is observed as the O_2 concentration is increased. Consequently, if mass loss is the primary quantity of interest, use of CCK is recommended over using LH as long as the ultimate analysis of the coal considered yields a C > 80%, since the correlations much below this threshold are unreliable given the results shown in Fig. 2.

Comparison of devolatilization models demonstrates that use of CPD yields more accurate predictions for particle mass than the TS model. This is primarily because the TS model predicts that a larger fraction of the coal mass is devolatilized than what is predicted by CPD. As a result, CPD is recommended if accurate predictions of particle mass are required. Furthermore, temperature predictions tend to be slightly lower when the TS model is used over CPD. This appears to be caused by the different speciations predicted by either model. For both CPD and TS, it was found that there was a significant overlap between devolatilization and char oxidation, which suggests that the assumption that surface reactions occur only with amorphous carbon is likely violated during the earlier stages of char oxidation. The predicted overlap of char oxidation and devolatilization is relatively short-lived for the cases considered so it doesn't have a substantial long-term effect on particle mass calculations. However, the same may not be true for systems with lower ambient O_2 concentrations and thus warrants further investigation.

Varying initial furnace temperature did not have a substantial effect on the behavior of particle temperature or mass histories calculated by either char model considered. Sensitivity to $T_{g,0}$ was greatest for cases in which the O_2 concentration was 6%, and decreased as the O_2 increased. This is because combustion of devolatilized matter occurs closer to the particle because char oxidation occurs to a larger extent in high oxygen environments.

Varying initial particle diameter had a significant impact on both temperature and burnout calculations, as expected, with the rate of char burnout increasing with decreasing particle diameter for both the CCK and LH models. Evolution of particle temperature histories with changing $d_{p,0}$ is more interesting. At O_2 concentrations, particle temperature tends to decrease with increasing $d_{p,0}$ for both char reaction models implemented. However, this trend begins to reverse as the fraction of O_2 is increased, and completely reverses at 36% O_2 when the LH model is used for burnout calculations. This observation due largely to the scaling behavior of source terms for the particle temperature.

Acknowledgments

This material is based upon work supported by the Department of Energy, National Nuclear Security Administration, under Award Number(s) DE-NA0002375.

References

[1] Watanabe H, Otaka M. Numerical simulation of coal gasification in entrained flow coal gasifier. Fuel 2006;85(12–13):1935–43.
[2] Schuhbauer C, Angerer M, Spliethoff H, Kluger F, Tschaffon H. Coupled simulation of a tangentially hard coal fired 700 °C boiler. Fuel 2014;122:149–63.
[3] Wang X, Jin B, Zhong W. Three-dimensional simulation of fluidized bed coal gasification. Chem Eng Process: Process Intens 2009;48(2):695–705.
[4] Askarova AS, Messerle VE, Ustimenko AB, Bolegenova SA, Maximov VY, Gabitova ZK. Numerical simulation of pulverized coal combustion in a power boiler furnace. High Temp 2015;53(3):445–52.
[5] Murphy JJ, Shaddix CR. Combustion kinetics of coal chars in oxygen-enriched environments. Combust Flame 2006;144(4):710–29.
[6] Kim D, Choi S, Shaddix CR, Geier M. Effect of CO_2 gasification reaction on char particle combustion in oxy-fuel conditions. Fuel 2014;120:130–40.
[7] Hurt R, Sun J-K, Lunden M. A kinetic model of carbon burnout in pulverized coal combustion. Combust Flame 1998;113(1–2):181–97.
[8] Niksa S, Liu GS, Hurt RH. Coal conversion submodels for design applications at elevated pressures. Part I. Devolatilization and char oxidation. Prog Energy Combust Sci 2003;29(5):425–77.
[9] Liu GS, Niksa S. Coal conversion submodels for design applications at elevated pressures. Part II. Char gasification. Prog Energy Combust Sci 2004;30(6):679–717.
[10] Shurtz RC. Effects of pressure on the properties of coal char under gasification conditions at high initial heating rates, PhD thesis; 2011. <http://scholarsarchive.byu.edu/etd/2877/>.
[11] Shurtz RC, Fletcher TH. Coal Char-CO_2 gasification measurements and modeling in a pressurized flat-flame burner. Energy Fuels 2013;27(6):3022–38.
[12] Hecht ES, Shaddix CR, Molina A, Haynes BS. Effect of CO_2 gasification reaction on oxy-combustion of pulverized coal char. Proc Combust Inst 2011;33(2):1699–706.
[13] Liu Y, He R. Modeling of the pore structure evolution in porous char particles during combustion. Combust Sci Technol 2016;188(2):207–32.
[14] Maloney DJ, Monazam ER, Casleton KH, Shaddix CR. Evaluation of char combustion models: measurement and analysis of variability in char particle size and density. Proc Combust Inst 2005;30(2):2197–204.
[15] Gonzalo-Tirado C, Jiménez S, Johansson R, Ballester J. Comparative study of four alternative models for CO oxidation around a burning coal char particle. Combust Flame 2014;161(4):1085–95.
[16] Goshayeshi B, Sutherland JC. A comparison of various models in predicting ignition delay in single-particle coal combustion. Combust Flame 2014;161(7):1900–10.
[17] Biagini E, Tognotti L. Comparison of devolatilization/char oxidation and direct oxidation of solid fuels at low heating rate. Energy Fuels 2006;20(3):986–92.
[18] McConnell J, Sutherland JC. The effect of model fidelity on prediction of char burnout for single-particle coal combustion. Proc Combust Inst 2016. 9999–9999.
[19] Lewis AD, Holland TM, Marchant NR, Fletcher EG, Henley DJ, Fuller EG, et al. Steam gasification rates of three bituminous coal chars in an entrained-flow reactor at pressurized conditions. Energy Fuels 2015;29(3):1479–93.
[20] Lewis AD, Fletcher EG, Fletcher TH. CO_2 gasification rates of petroleum coke in a pressurized flat-flame burner entrained-flow reactor. Energy Fuels 2014;7(8):4447–57.
[21] Lewis AD, Fletcher EG, Fletcher TH. CO_2 char gasification rates of sawdust, switchgrass, and corn stover in a pressurized entrained-flow reactor. Energy Fuels 2014;9(9):5812–25.
[22] Goshayeshi B, Sutherland JC. Prediction of oxy-coal flame stand-off using high-fidelity thermochemical models and the one-dimensional turbulence model. Proc Combust Inst 2015;35(3):2829–37.
[23] Ming-yan G, Ming-chuan Z, Juan Y, Wei-dong F, Feng-guo T. Numerical study on the spatial distribution of energy release during char combustion. Appl Energy 2008;85:1060–70.
[24] Goshayeshi B, Mcconnell J, Sutherland JC. An improved model for heat transfer at particle surfaces during heterogeneous char combustion. In: Western States Section of the Combustion Institute, Seattle, WA. 2016. p. 1–14.
[25] Slavinskaya N, Braun-Unkhoff M, Frank P. Reduced reaction mechanisms for methane and syngas combustion in gas turbines. J Eng Gas Turb Power 2008;130(2):021504.
[26] Brown AL, Fletcher TH. Modeling soot derived from pulverized coal. Energy Fuels 1997;4(12):745–57.
[27] Kobayashi H, Howard J, Sarofim A. Coal devolatilization at high temperatures. Symp (Int) Combust 1977;16(1):411–25.
[28] Fletcher TH, Kerstein AR, Pugmire RJ, Solum M, Grant DM. A chemical percolation model for devolatilization: summary. Tech rep, Combustion Research Facility, Sandia National Laboratories; 1992.
[29] Bhatia SK, Perlmutter DD. A random pore model for fluid-solid reactions: I. Isothermal, kinetic control. AIChE J 1980;26(3):379–86.
[30] Mitchell RE. Variations in the temperatures of coal-char particles during combustion: a consequence of particle-to-particle variations in ASH-content. Symp (Int) Combust 1991;23(1):1297–304.
[31] Tognotti L, Longwell J, Sarofim A. The products of the high temperature oxidation of a single char particle in an electrodynamic balance. Symp (Int) Combust 1991;23(1):1207–13.
[32] Sutherland JC, Kennedy CA. Improved boundary conditions for viscous, reacting, compressible flows. J Comput Phys 2003;191(2):502–24.
[33] Sutherland J, Punati N, Kerstein AR. A unified approach to the various formulations of the one-dimensional-turbulence model. Tech rep, Institute for Clean Secure Energy; 2010.
[34] Mulcahy MFR. Gas kinetics. Wiley; 1973.
[35] Shaddix C. Personal communication; March 18, 2016.
[36] Hecht ES, Shaddix CR, Lighty JS. Analysis of the errors associated with typical pulverized coal char combustion modeling assumptions for oxy-fuel combustion. Combust Flame 2013;160(8):1499–509.